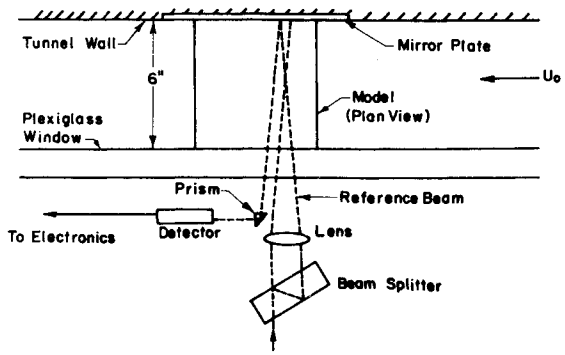

Fig. 1 Experimental geometry.

The hydrofoil model used in this test was an NACA 66-210 profile with a chord of 6 in. At a typical freestream velocity of 30 fps, the boundary layer thickness at the trailing edge is about 0.12 in. and the chord Reynolds number is 1.5×10^6. The pressure surveys were made by positioning the LDV measuring volume at the desired distance (x) from the leading edge, and then increasing the distance (y) from the wall until just outside of the boundary layer. The outer edge of this thin boundary layer was easy to locate by the sudden decrease in the turbulence level as detected by the LDV. Outside of the boundary layer the velocity was found to be a relatively weak function of y. At each measurement point the velocity was averaged over a 10 sec period, and the scatter of the results was about 0.3%. (This scatter, although small, might be further reduced by replacing the Plexiglas test section window with one of better optical quality.)

III. Results and Conclusions

Pressure distributions on the NACA profile were measured for angles of attack of 0, 3, and 6°. Values of $(U/U_o)^2$ were plotted by computer and are shown in Fig. 2. These results are in reasonable agreement with theoretical predictions for this airfoil shape.[4] Further tests of this technique will include lift and drag measurements on the model which will be compared to the forces predicted from the pressure distributions.

This method of measuring surface pressure distributions has several advantages which make it a desirable alternative to the pressure tap model. Most obvious is the fact that the models are much less expensive and easier to build. Pressure tap models are completely impossible in some cases, such as the present generation of supercavitating hydrofoils with very sharp leading edges. Another advantage is that pressure measurements can be made at as many values of x as desired using the LDV technique, whereas the number of points for a pressure tap model is very limited and points cannot be spaced more closely in regions of interest. In addition, pressure tap models have an artificial surface roughness which may itself affect the pressure distribution.

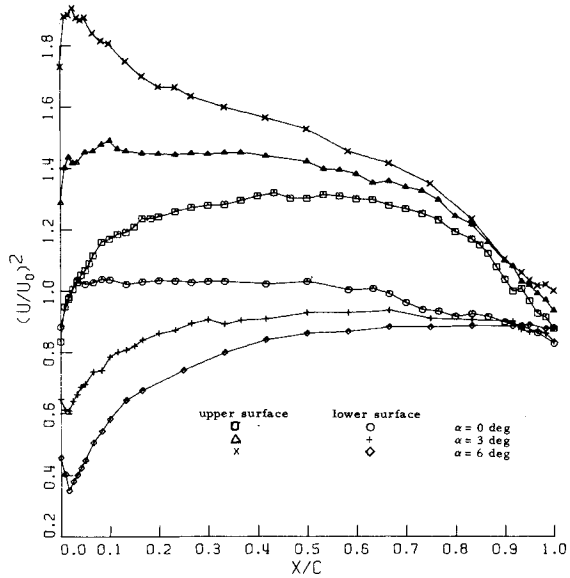

Fig. 2 Surface pressure distributions.

The method described here is of course subject to the assumptions inherent in the equation $p+\frac{1}{2}\rho U^2 = \text{constant}$, and the assumption of constant pressure across the boundary layer. This latter assumption requires that boundary layers remain thin and attached; separated flows are not considered. However, for the testing of almost any thin wing or hydrofoil section, these assumptions are not restrictive. In flows over more complex shapes where separation could occur, the LDV measurements should be supported by conventional surface pressure measurements.

If the LDV technique is to be used as a standard testing procedure, it is expected that the traversing over a contour and recording of velocities will be automated. At Caltech a small, on-line computer will be used to generate the required x-y coordinates for the survey, and the traversing mechanism will be driven to these coordinates by stepper motors. The computer will then record the LDV frequencies and generate a plot of $(U/U_o)^2$. In this way it should be possible to survey a model surface in a couple of minutes of tunnel time.

References

[1] Knapp, R. and Levy, J., "The Hydrodynamics Laboratory of the California Institute of Technology," *Transactions of the American Society of Mechanical Engineers*, Vol. 70, July 1948, p. 437.

[2] Barker, S. J., "Laser-Doppler Measurements on a Round Turbulent Jet in Dilute Polymer Solutions," *Journal of Fluid Mechanics*, Vol. 60, Pt. 4, Oct. 1973, p. 721.

[3] Baker, G. R., Barker, S. J., Bofah, K. K., and Saffman, P. G., "Laser Anemometer Measurements of Trailing Vortices in Water," *Journal of Fluid Mechanics*, Vol. 65, Pt. 2, Aug. 1974, p. 325.

[4] Abbott, I., et al., "Summary of Airfoil Data," Rept. 824, 1945, NACA.

Independent Region of Acceleration in Solid Propellant Combustion

TAKASHI NIIOKA* AND TOHRU MITANI*
National Aerospace Laboratory, Miyagi, Japan

Introduction

THE spinning of a rocket causes a marked change in the performance of the solid propellant rocket, and that change is unpredictable from the motor at rest. Usually, the chamber pressure is higher, the burning time is shorter, and the total impulse is lower, respectively, than those in the similar motor fired under static condition. These differences are due to the increases in the burning rate augmentation in the radial acceleration field. The burning rate, however, keeps its value constant up to certain acceleration (here referred to as "critical acceleration"), and under certain circumstances the spinning rocket motor may be designed in the independent region of acceleration, should the rocket performance be different from the one of the static condition. The purpose of the present study is to investigate the pressure dependence of the critical acceleration, especially concentrating our effort on the comparison of the composite propellant with CMDB (Composite Modified Double-Base) propellant.

Received May 20, 1974.
Index category: Fuels and Propellants, Properties of.

* Research Engineer, Kakuda Branch.

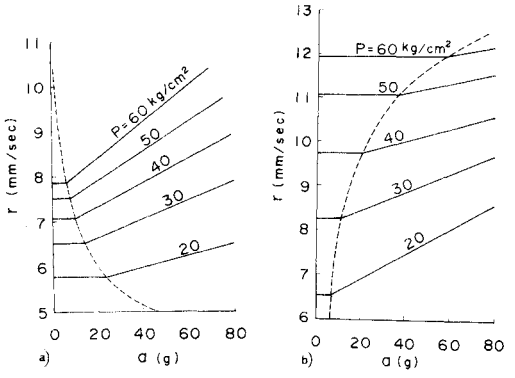

Fig. 1 Acceleration sensitivity of two kinds of propellants: a) composite propellant (PB05); b) CMDB propellant (CD07).

Experimental Procedure and Propellants

In an attempt to minimize the effects of propellant geometry, the nearly undirectional burning slab motors were fired on a centrifuge at acceleration loads varied from 0 g to 350 g. The propellant slab of 50 mm × 100 mm × 15 mm was coated by an inhibitor material against five sides and inserted into the slab motor, and the centrifuge acceleration loads were directed vertically against the combustion surface. The test motors were fired at pressure levels from 20 kg/cm^2 to 80 kg/cm^2 by changing the nozzle throat area for each acceleration level. The burning rate data obtained from each acceleration test were plotted on a logarithmic graph paper and were fit to Vieille's burning rate rule by means of the least squares method. The intersection of the straight line at any acceleration and the one at 0 g is the critical point.

Composite propellants (PB) composed of ammonium perchlorate (83.7%) and carboxy-terminated polybutadiene (16.3%), and CMDB propellants composed of nitroglycerine (33.6%), nitrocellulose (28.0%), ammonium perchlorate (30.0%), and plasticizer (8.4%) were used in this study. Twenty-one combinations of propellant were arranged by several kinds of the aluminum mass median diameter and the aluminum content. The detailed composition is found in Refs. 1 and 2 reported by the authors.

Results and Discussion

The burning rate (r) is calculated from Vielle's rule at each pressure as shown in Fig. 1. PB05 and CD07 propellant contain 9% and 9.1% aluminum, respectively. In the case of composite propellants, the increase in the pressure level induces narrower region independent of acceleration. The variation of the burning rate in the affected region gives almost straight line in the low acceleration field, and the burning rate augmentation is increased as the pressure is increased. On the other hand, the CMDB propellant is in contrast to the composite propellant. When rearranging the experimental results, these may be summarized in Fig. 2, and the outline of the discussion of this contrast is as follows.

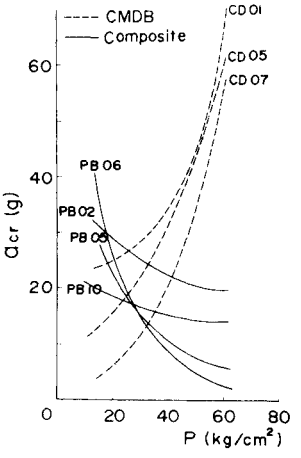

Fig. 2 Comparison of critical acceleration vs pressure for composite propellants and CMDB propellants.

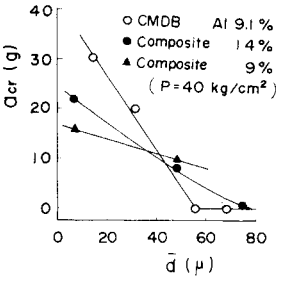

Fig. 3 The effect of aluminum mass median diameter on critical acceleration.

An analytical model is developed on the basis of Crowe and Willoughby study[3] that metal particles are retained on the combustion surface by a centrifugal force field and become a heat source responsible for an increased burning rate. Hence the critical acceleration is determined by using the Stoke's law for the drag coefficient as follows,

$$a_{cr} = 18 r_o \rho_s (1-w) \mu_g / \rho_g \rho_{al} \bar{d}^2 \tag{1}$$

where a_{cr} is the critical acceleration, r_o the burning rate at 0 g, w the aluminum content, μ_g the viscosity, $\bar{d}$ the mass median diameter of aluminum, ρ_s the density of propellant, ρ_g the density of combustion gases, and ρ_{al} the density of aluminum. The parameters dependent on pressure are r_o, ρ_g, and μ_g. By substituting $r_o \sim P^n$, $\rho_g \sim P$, and $\mu_g \sim P^m$ and differentiating Eq. (1)

$$da_{cr}/dp \sim (m+n-1)P^{m+n-2} \tag{2}$$

is obtained. At the high pressure $d\mu_g/dp > 0$, i.e., $m > 0$ holds for μ_g, and m is approximately $0.6 \sim 0.65$ for the experimental pressure.[4] Accordingly, $da_{cr}/dp < 0$ for composite propellants ($n = 0.25 \sim 0.35$) and $da_{cr}/dp > 0$ for CMDB propellants ($n = 0.4 \sim 0.58$) are obtained and then the experimental results can be explained. Furthermore the fact that the increasing pressure exponent induces a lower gradient curve for the composite propellant and a higher gradient for the CMDB propellant in Fig. 2, agrees with the analytical results of Eq. (2).

The aluminum diameter may have a strong effect on the critical acceleration as shown in Eq. (1). As it is clear in Fig. 3 with the aluminum diameter as the axis of abscissa, the critical acceleration is reduced as the particle diameter is increased. However, the effect of the aluminum content is very complex and there is no general tendency in the variation of the burning rate augmentation with the acceleration.[2] The effect of the change in the basic burning rate (r_o) with aluminum content may be considered the reason for this complicated aspect.

Conclusion

The contrast between the composite propellants and the CMDB propellants was found in the pressure dependence of the critical acceleration, but below that the burning rate augmentation was not observed. The combustion of the composite propellants in the acceleration field is more sensitive to high pressure, and the CMDB propellants are completely contrary to this. It is evident that more work using different approaches, for example, the difference of the combustion mechanism between two kinds of propellant, is needed.

References

[1] Ishii, S., Niioka, T., and Mitani, T., "An Analytical and Experimental Study for Solid Propellant Combustion in an Acceleration Field," *Combustion Science and Technology*, Vol. 8, No. 4, 1974, p. 177.

[2] Ishii, S., Niioka, T., and Mitani, T., "Combustion of Composite Propellants in Acceleration Field," TR-354, 1974, National Aerospace Laboratory, Miyagi, Japan.

[3] Crowe, C. T. and Willoughby, P. G., "Effect of Spin on the Internal Ballistics of a Solid Propellant Motor," AIAA Paper 66-523, Los Angeles, Calif., 1966.

[4] Enskog, D., "Kinetische Theorie der Warmeleitung, Reibung und Selbstdiffsion in gewissen verdichteten Gasen und Flussigkeiten," *Svenska Vetenskapsakademiens Handl.*, Vol. 63, No. 4, 1922, pp. 44S.

New Triangular Plate-Bending Finite Element with Transverse Shear Flexibility

R. NARAYANASWAMI*

NASA Langley Research Center, Hampton, Va.

Introduction

EARLY formulations of triangular plate-bending finite elements were given by Clough and Tocher[1] and by Bazeley et al.[2] Improvements to these elements have been made by using higher degree polynomials for transverse displacements; indeed elements of very high accuracy have been reported by Argyris,[3] Bell,[4] and Cowpoer et al.[5] using quintic polynomials for the displacement field. These high accuracy elements, however, have curvatures and/or higher order derivatives of displacements as grid point degrees of freedom. This situation leads to an inconvenience when step property variations are introduced. Furthermore, the elements discussed in Refs. 1–5 do not possess the property of transverse shear flexibility. Clough and Felippa[6] and Irons and Razzaque[7] have included the effects of transverse shear flexibility in finite element formulations without additional degrees of freedom to control transverse shear. The elements of Refs. 6 and 7, however, have w, $w_{,x}$, and $w_{,y}$ as grid point degrees of freedom rather than the quantities w, θ_x and θ_y required for continuity and proper treatment of boundary conditions in the presence of transverse shear.

The purpose of this Note is to describe a new triangular plate-bending finite element that has the advantages of the accuracy associated with a high-order displacement polynomial but does not have the previously discussed disadvantages and therefore is suitable for inclusion in general-purpose computer programs. The element has 18 degrees of freedom: the transverse displacement and 2 rotations at each vertex and at the midpoint of each side. Only displacements and rotations are included as grid point degrees of freedom and a quintic polynomial is used for lateral displacement. Effects of transverse shear have been taken into account in the element formulation by a procedure based on that used in NASTRAN[8] and a similar work for a quartic element communicated to the author by MacNeal.[9] The components of transverse shear strain are quadratic functions of position. Convergence to the limiting case of zero transverse shear strain is uniform.

Two problems of plate bending are analyzed using the new triangular elements, the static and free vibration analysis of a square isotropic plate with all edges 1) simply supported and 2) clamped. Results of calculations for displacements and stresses are compared with exact solutions from classical plate theory and with other available finite element solutions from the literature. Good accuracy is achieved with the new element for practical mesh subdivisions. In addition, two examples are presented which demonstrate the ability of the element to model the effects of transverse shear deformation in moderately thick to thick isotropic plates. Comparisons with 3-D elasticity solutions indicate the adequacy of the modeling of transverse shear in isotropic plates shown herein.

Received May 20, 1974; revision received July 26, 1974.

Index categories: Structural Static Analysis; Structural Dynamic Analysis.

* NASA-NRC Resident Research Associate.

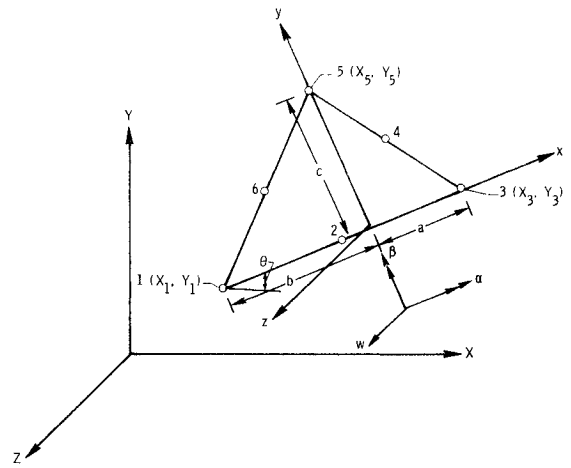

Fig. 1 Geometry of triangular element.

Derivation of Element Properties

Element geometry

A typical triangular element is shown in Fig. 1, where X, Y, and Z comprise a system of global coordinates and x, y, z comprise the system of local coordinates. The grid points of the element are numbered in counterclockwise direction as shown. The relationship between the dimensions of the triangular element a, b, c, the inclination θ between the global and local axes and the coordinates of the vertices of the element can be easily derived.[10,11]

Displacement field

The deflection $w(x, y)$ within the triangular element is assumed to vary as a quintic polynomial in the local coordinates; i.e.,

$$w(x,y) = a_1 + a_2x + a_3y + a_4x^2 + a_5xy + a_6y^2 + a_7x^3 + a_8x^2y + a_9xy^2 + a_{10}y^3 + a_{11}x^4 + a_{12}x^3y + a_{13}x^2y^2 + a_{14}xy^3 + a_{15}y^4 + a_{16}x^5 + a_{17}x^4y + a_{18}x^3y^2 + a_{19}x^2y^3 + a_{20}xy^4 + a_{21}y^5 \quad (1)$$

There are 21 independent coefficients a_1–a_{21}. These are evaluated as follows: the element has 18 degrees of freedom; viz, w, displacement in z direction; α, rotation about the x axis; and β, rotation about y axis at each of the 6 grid points. The rotations α and β are geometrically related to transverse shear strains γ_{xz} and γ_{yz} by

$$\gamma_{xz} = \partial w/\partial x + \beta \quad (2)$$

$$\gamma_{yz} = \partial w/\partial y - \alpha \quad (3)$$

It is shown in Ref. 11 that α and β can also be conveniently related to γ_{xz} and γ_{yz} through the moment equilibrium equations:

$$V_x + \partial M_x/\partial x + \partial M_{xy}/\partial y = 0 \quad (4)$$

$$V_y + \partial M_y/\partial y + \partial M_{xy}/\partial x = 0 \quad (5)$$

and, hence, can be expressed in terms of the coefficients a_1–a_{21}. Thus, 18 equations relating w, α, and β at the grid points to the 21 constants are obtained. Three additional relations are obtained by imposing the conditions that the edge rotation varies cubically along each edge.[5] Thus, the 21 coefficients can be uniquely determined in terms of the element nodal displacement vector. There is no rotation continuity between adjacent elements